

Geometries and properties of excited states in the gas phase and in solution: Theory and application of a time-dependent density functional theory polarizable continuum model

Giovanni Scalmani, Michael J. Frisch, Benedetta Mennucci, Jacopo Tomasi, Roberto Cammi, and Vincenzo Barone

Citation: *The Journal of Chemical Physics* **124**, 094107 (2006); doi: 10.1063/1.2173258

View online: <http://dx.doi.org/10.1063/1.2173258>

View Table of Contents: <http://scitation.aip.org/content/aip/journal/jcp/124/9?ver=pdfcov>

Published by the AIP Publishing

Articles you may be interested in

Phosphorescence lifetimes of organic light-emitting diodes from two-component time-dependent density functional theory

J. Chem. Phys. **141**, 224302 (2014); 10.1063/1.4902013

Implementation of the analytic energy gradient for the combined time-dependent density functional theory/effective fragment potential method: Application to excited-state molecular dynamics simulations

J. Chem. Phys. **134**, 054111 (2011); 10.1063/1.3523578

Excited state geometry of photoactive yellow protein chromophore: A combined conductorlike polarizable continuum model and time-dependent density functional study

J. Chem. Phys. **133**, 034108 (2010); 10.1063/1.3462248

A state-specific polarizable continuum model time dependent density functional theory method for excited state calculations in solution

J. Chem. Phys. **125**, 054103 (2006); 10.1063/1.2222364

Two-photon absorption in solution by means of time-dependent density-functional theory and the polarizable continuum model

J. Chem. Phys. **122**, 244104 (2005); 10.1063/1.1944727



NEW Special Topic Sections

NOW ONLINE
Lithium Niobate Properties and Applications:
Reviews of Emerging Trends

AIP Applied Physics Reviews

Geometries and properties of excited states in the gas phase and in solution: Theory and application of a time-dependent density functional theory polarizable continuum model

Giovanni Scalmani^{a)} and Michael J. Frisch
Gaussian, Inc., Wallingford, Connecticut 06492

Benedetta Mennucci and Jacopo Tomasi
Dipartimento di Chimica, Università di Pisa, Via Risorgimento 35, 56126 Pisa, Italy

Roberto Cammi
Dipartimento di Chimica, Università di Parma, Viale delle Scienze 17/A, 43100 Parma, Italy

Vincenzo Barone
Dipartimento di Chimica, Università di Napoli Federico II, Complesso Universitario di Monte Santangelo, Via Cintia, I-80126 Napoli, Italy

(Received 21 November 2005; accepted 17 January 2006; published online 3 March 2006)

In this paper we present the theory and implementation of analytic derivatives of time-dependent density functional theory (TDDFT) excited states energies, both *in vacuo* and including solvent effects by means of the polarizable continuum model. The method is applied to two case studies: p-nitroaniline and 4-(dimethyl)aminobenzonitrile. For both molecules PCM-TDDFT is shown to be successful in supporting the analysis of experimental data with useful insights for a better understanding of photophysical and photochemical pathways in solution.

© 2006 American Institute of Physics. [DOI: [10.1063/1.2173258](https://doi.org/10.1063/1.2173258)]

I. INTRODUCTION

The time-dependent formulation of density functional theory, widely known as TDDFT, is an exact quantum mechanical theory in which the time-dependent density is the fundamental variable and the exchange-correlation (XC) potential describes the many-body interactions.¹ For small changes in the time-dependent XC potential, the linear response approach can be applied to solve the TDDFT equations. In this way it is possible to obtain the relative energies of the excited states (the excitation energies) as poles of the frequency dependent ground state linear response function.² Due to its good accuracy and its reasonable computational cost, in the last several years, TDDFT has replaced Hartree-Fock-based single-excitation theories (CIS) as the method of choice for the calculation of valence excitation energies in medium to large sized molecules. Indeed, TDDFT provides a fast and reliable approach to obtain potential energy surfaces for the excited states as a function of the molecular geometry by simply adding the ground state DFT energy to the excitation energy of the selected state. In addition, the excited state first order properties (forces on the nuclei, electric multipole moments,...) can be expressed via Helman-Feynman theorem, as the first derivatives (gradients) of the excited state energy with respect to suitable external perturbations.³ In this framework the availability of analytical TDDFT gradients plays a strategic role in reducing the computational effort required by the exploration of the excited states potential energy surface (PES).

Van Caillie and Amos pioneered this field⁴ formulating

the theory of analytical geometrical derivatives for TDDFT using local density approximation (LDA), gradient corrected and hybrid functionals. More recently, Furche and Ahlrichs⁵ have presented the theory, the implementation, and the validation of several excited state properties obtained from the TDDFT. Their approach is based on a fully variational formulation for the excited state energy functional which allows for a very compact derivation of the first order properties, geometrical derivatives, and electronic density multipolar expansion. Benchmark results using hybrid functionals showed that structural properties of excited states are almost as accurate as those of the ground state calculations, at a comparable computational cost, even for fairly large molecules. In all these examples, however, an important aspect has not been considered, namely, the inclusion of solvent effects; until now, in fact, the TDDFT gradients have been limited to isolated molecules and this despite the fact that a large part of the experiments probe excited states of molecules in solution. This work presents the theory and the implementation of the analytical TDDFT gradients for the molecules in solution within the framework of the polarizable continuum model (PCM).^{17,19} There are several versions of PCM, characterized by the particular choice of electrostatic boundary conditions: Dielectric PCM (DPCM) (Ref. 6) and Integral equation formalism PCM (IEFPCM) (Ref. 7) involve dielectric boundary conditions, while CPCM (Refs. 8 and 9) from the conductor-like ones. Among these methods, IEFPCM is by far the most general since it can model with consistent accuracy not only isotropic solvents (with both high and low dielectric constant), but also anisotropic solvents¹⁰ and ionic solutions.¹¹ Our derivation of the PCM-TDDFT gradient is

^{a)}Electronic mail: giovanni@gaussian.com

carried out on the same line originally used¹² by three of the present authors for the PCM-CIS gradients, but relies on the most up-to-date PCM formalism and implementation technology.

The introduction of a solvent makes the description of excited states an extremely complex problem; many new aspects have, in fact, to be considered in addition to those already present in the case of isolated systems. Here, in particular, we deal with two aspects of the study of excited states in solution, common to all the linear response schemes such as CIS, time-dependent Hartree-Fock (TDHF), and TD-DFT, and regarding the definition of the energies of the excited states (and thus affecting also their derivatives and properties). Note that for our purposes in this paper, we consider CIS as a linear response method, rather than a truncated CI method, because it can be seen as a simplification of TDHF (by setting the **B** matrix to zero, *vide infra*).

The first aspect is related to the fact that the electronic excitation is a process involving not only the solute but the entire solute-solvent system. As a consequence, the definition of the excited states of molecular solutes requires also the characterization of the solvent degrees of freedom. The difference of the characteristic time scale of the electronic degrees of freedom of the solute and the composite degrees of freedom of the solvent may lead to different excited state regimes, with two extreme situations (i) the “nonequilibrium regime” in which the slow degrees of freedom of the solvent are not equilibrated with the excited state electronic redistribution upon excitation (vertical excitation processes), and (ii) the “equilibrium regime” in which the solvent is allowed to equilibrate (i.e., reorganize) all its degrees of freedom including the slow ones. The different regimes may dramatically influence the properties of the solute excited states, and the analytical derivatives algorithm should allow for the use of such different solvation regimes.

The second aspect concerns the status of the excitation energies of a solvated system. In a recent paper,¹³ we have shown the intrinsic differences between the linear response (TDHF, CIS, and TDDFT) and state specific approaches [complete active space self-consistent field (CASSCF), CI,...] in the computation of excitation energies in the framework of quantum mechanical (QM) continuum solvation models. The state specific approaches, which are based on the explicit calculation of the excited state wave function, described in a more satisfactory way the variation of the solute-solvent interaction accompanying the change of the electronic density during an electronic excitation. On the other hand, the linear response methods introduce only effects related to the corresponding transition density. However, the calculations performed on the model chromophores have also shown that these differences have usually little effect on the excitation energies computed within the two different schemes. In addition, this intrinsic limit of linear response excited states energies with respect to the state specific methods should have a less relevant effect when the derivatives of the excited states energies are considered since cancellation of errors may occur.

We conclude this short introduction by mentioning, for the sake of completeness, two other methods using analytical derivatives for the excited state energy in a time-dependent formalism and taking into account solvent effects. The first is the collective electronic oscillator (CEO) method developed by Mukamel and co-workers¹⁴ for the semiempirical INDO/S Hamiltonian which includes a solvation contribution in terms of a spherical Onsager continuum model. The second¹⁵ is a Car-Parrinello molecular dynamics (CPMD) scheme,¹⁶ which describes the *ab initio* molecular dynamics of an electronically excited system within the TDDFT random-phase (RP) approximation and includes the solvation effects in terms of explicit solvent molecules. The CEO method may be viewed as an approach best suited for applications to large systems in order to get a qualitative estimate of the solvent effects, while CPMD represents a possible strategy towards a more complete description of solvation.

The paper is organized in two main parts, in the first one, the theory of the TDDFT gradients is presented for both isolated and solvated systems whereas in the second part, two studies of excited state geometries and properties are presented for **paranitroaniline** (PNA) and 4-(dimethyl)aminobenzonitrile (DMABN) in gas phase and in cyclohexane and acetonitrile solutions. These two studies are presented here to show how the theory of TDDFT gradients for solvated systems can be applied to the analysis of UV spectra and to understand photophysical and photochemical pathways.

II. THEORY

A. The basic PCM theory

The polarizable continuum model⁶ (PCM) describes the solvent as a structureless continuum, characterized by its dielectric permittivity ϵ , in which a molecular-shaped empty cavity is dug to host the solute which is fully described by its QM charge distribution. The dielectric medium is polarized by the solute charge distribution and acts as the source of a reaction field which in turn polarizes back the solute. This mutual effect is evaluated by solving the proper electrostatic problem described by the Poisson and Laplace equations with the proper boundary conditions at the cavity surface.¹⁷⁻¹⁹

As noted in the Introduction, nowadays, the acronym PCM indicates a family of methods which can be distinguished on the basis of the boundary conditions and the numerical approach used to solve the Poisson-Laplace electrostatic problem. In all formulations of PCM, the polarization of the medium is represented by the solvent reaction field expressed in terms of a potential defined through an apparent charge distribution, σ , spread on the cavity surface. The most general and powerful version of PCM, i.e., IEFPCM, is based on the use of proper Green functions, defined inside and outside the cavity, to compute the integral operators defining the apparent charge σ . This allows for the application of the same formalism to a very different media: from standard isotropic solvents characterized by a scalar permittivity, to anisotropic dielectrics such as liquid crystals and polymers, to liquid-liquid, liquid-gas, and liquid-solid interfaces.

Details on the formal derivation of the model as well as the exact expression of the integral operators defining σ can be found in Ref. 7 and will not be repeated here.

The generalization of this model to include a QM description of the solute charge calls for the definition of an effective Hamiltonian, i.e., a Hamiltonian to which the solute-solvent interactions are added in terms of a solvent reaction operator

$$H_{\text{eff}}|\Psi\rangle = [H^0 + V^{\text{PCM}}]|\Psi\rangle = E|\Psi\rangle, \quad (1)$$

where H^0 is the Hamiltonian describing the isolated molecule, and V^{PCM} is the QM analog of the solvent reaction potential. The treatment of the operator V^{PCM} is delicate, as it depends on the solute total density (through the apparent charges) inducing a nonlinear character in the solute Schrödinger equation. Such an equation can be solved with all the techniques developed for isolated systems. It is, however, important to note that now the correct energetic quantity to consider is the free energy functional,

$$\mathcal{G} = E + \frac{1}{2}\langle\Psi|V^{\text{PCM}}|\Psi\rangle. \quad (2)$$

The \mathcal{G} functional has a privileged role in the theory, as the solution of the Schrödinger equation gives a minimum of this functional even though it is not the eigenvalue of the nonlinear Hamiltonian, here indicated as E . The difference between E and \mathcal{G} has, however, a clear physical meaning, it represents the polarization work done by the solute to create the charge density inside the solvent. It is worth noting that this interpretation is equally valid for zero-temperature models and for those in which the thermal agitation is implicitly or explicitly taken into account.

Within a DFT framework, the molecular Kohn-Sham (KS) operator thus becomes a sum of the core Hamiltonian h , a Coulomb and (scaled) exchange term, the exchange-correlation potential V^{xc} , and the solvent reaction operator V^{PCM} of Eq. (1), namely,

$$F_{pq\sigma} = h_{pq\sigma} + \sum_{i\sigma'} [(pq\sigma|ii\sigma') - c_x \delta_{\sigma\sigma'}(pi\sigma|i q\sigma)] + V_{pq\sigma}^{\text{xc}} + V_{pq\sigma}^{\text{PCM}}, \quad (3)$$

where $(pq\sigma|ii\sigma')$ is a two-electron repulsion integral in the Mulliken notation and

$$V_{pq\sigma}^{\text{xc}} = \frac{\partial E^{\text{xc}}}{\partial P_{pq\sigma}}$$

being P the ground state density matrix [indices i, j, \dots label occupied, a, b, \dots virtual, and p, q, \dots generic molecular orbital (MO) whereas σ, σ' are spin labels]. In Eq. (3) we have used the hybrid mixing parameter c_x originally introduced by Becke²⁰ which allows us to interpolate between the limits of “pure” density functionals ($c_x=0$, no “exact” exchange) and HF theory ($c_x=1$, full exchange and $E^{\text{xc}}=0$).⁵

The solvent induced term $V_{pq\sigma}^{\text{PCM}}$ represents the electrostatic interaction between the solvent apparent charge σ and the solute’s nuclei and electrons. In the computational practice a boundary-element method (BEM) is applied by partitioning the cavity surface into discrete elements, called *tesserae*, and by substituting the apparent charge σ by a col-

lection of point charges q_k , each one placed at the center of a tessera \mathbf{s}_k . We thus obtain

$$q_k = \sum_l \mathbf{Q}_{kl} V_l. \quad (4)$$

The detailed expression of the \mathbf{Q} matrix in Eq. (4) depends on the specific version of the PCM method being used and it has been previously published (see Ref. 19 for a complete survey), together with efficient ways to solve the associated linear system.²¹ Here we simply recall that the \mathbf{Q} matrix is determined by the form and shape of the cavity, by the details of the discretization of the surface and by the solvent permittivity ϵ .

As the matrix \mathbf{Q} is not symmetric, the correct expression of the solvent induced term $V_{pq\sigma}^{\text{PCM}}$ is obtained by introducing the symmetric analog of the matrix \mathbf{Q} , namely,

$$\mathbf{Q}^s = \frac{\mathbf{Q} + \mathbf{Q}^\dagger}{2},$$

where \mathbf{Q}^\dagger is the transpose. In such a way, the apparent charges q_k can be substituted by the so-called polarization weights, q_k^w ,²² and the solvent term becomes

$$V_{pq\sigma}^{\text{PCM}} = \sum_k V_{pq\sigma,k}^E q_k^w, \quad (5)$$

where $V_{pq\sigma,k}^E$ is the electronic electrostatic potential integral at the k th point on the cavity surface,

$$V_{pq\sigma,k}^E = - \int \psi_{p\sigma}^*(\mathbf{r}) \psi_{q\sigma}(\mathbf{r}) \frac{1}{|\mathbf{r} - \mathbf{s}_k|} d\mathbf{r}.$$

The polarization weights q_k^w are the solution of the symmetrized PCM linear system of equations:

$$q_k^w = \sum_l \mathbf{Q}_{kl}^s V_l, \quad (6)$$

where $V_k = V_k^N + V_k^E$ is the solute’s total electrostatic potential at the tesserae. The nuclear contribution V_k^N is trivially computed from the solute’s nuclear charge distribution while V_k^E is also easily computed in the atomic orbital (AO) basis from a generic one-particle density matrix \mathbf{P} as

$$V_k^E = - \sum_{\mu\nu\sigma} P_{\mu\nu\sigma} \int \chi_\mu^*(\mathbf{r}) \chi_\nu(\mathbf{r}) \frac{1}{|\mathbf{r} - \mathbf{s}_k|} d\mathbf{r},$$

where greek indices refer to AO basis functions.

B. Excitation energies within the PCM-TDDFT framework

In the linear response theory the excitation energies of a molecular system are determined as poles of the linear response function to a time-dependent perturbation.² They can thus be determined as the solution of the non-Hermitian eigensystem,²³

$$\begin{bmatrix} \mathbf{A} & \mathbf{B} \\ \mathbf{B} & \mathbf{A} \end{bmatrix} \begin{bmatrix} \mathbf{X} \\ \mathbf{Y} \end{bmatrix} = \omega \begin{bmatrix} 1 & 0 \\ 0 & -1 \end{bmatrix} \begin{bmatrix} \mathbf{X} \\ \mathbf{Y} \end{bmatrix}, \quad (7)$$

where the eigenvalue problem is of dimension $2N_{Occ}N_{Vir}$ and the vector $|\mathbf{X}, \mathbf{Y}\rangle$ are defined in the same Hilbert space²⁴ and are normalized as

$$[\mathbf{X} \ \mathbf{Y}] = \begin{bmatrix} 1 & 0 \\ 0 & -1 \end{bmatrix} \begin{bmatrix} \mathbf{X} \\ \mathbf{Y} \end{bmatrix} = 1. \quad (8)$$

The vectors $|\mathbf{X}, \mathbf{Y}\rangle$ represent the (frequency dependent) linear response of the density matrix in the basis of the unperturbed molecular orbitals; in particular, $\mathbf{X} = \delta P_{ia}(\omega)$ correspond to excitations, while $\mathbf{Y} = \delta P_{ai}(\omega)$ corresponds to deexcitation contributions. When the solvent effects are introduced according to the PCM model, the definition of the vectors $|\mathbf{X}, \mathbf{Y}\rangle$ does not change while the matrices \mathbf{A} and \mathbf{B} involve a separation into isolated-type and PCM-type potentials according to²⁵

$$A_{ai\sigma, bj\sigma'} = \delta_{ab}\delta_{ij}\delta_{\sigma\sigma'}(\epsilon_{a\sigma} - \epsilon_{i\sigma}) + (ia\sigma|jb\sigma') + f_{ai\sigma, bj\sigma'}^{\text{xc}} - c_x\delta_{\sigma\sigma'}(ab\sigma|ij\sigma) + \mathcal{V}_{ai\sigma, bj\sigma'}^{\text{PCM}}, \quad (9)$$

$$B_{ai\sigma, bj\sigma'} = (ia\sigma|jb\sigma') + f_{ai\sigma, bj\sigma'}^{\text{xc}} - c_x\delta_{\sigma\sigma'}(ja\sigma|ib\sigma) + \mathcal{V}_{ai\sigma, bj\sigma'}^{\text{PCM}}, \quad (10)$$

where $f_{ai\sigma, bj\sigma'}^{\text{xc}}$ represents a matrix element of the exchange-correlation kernel in the adiabatic approximation

$$f_{\sigma\sigma'}^{\text{xc}} = \frac{\partial^2 E^{\text{xc}}}{\partial \rho_{\sigma} \partial \rho_{\sigma'}}, \quad (11)$$

while $\mathcal{V}_{ai\sigma, bj\sigma'}^{\text{PCM}}$ is the corresponding matrix element of the PCM reaction potential which can be seen as a generalization of Eqs. (5) and (6),

$$\mathcal{V}_{ai\sigma, bj\sigma'}^{\text{PCM}} = \sum_{kl} V_{ai\sigma, k}^E Q_{kl}^S V_{bj\sigma', l}^E. \quad (12)$$

Equation (12) follows because in the current model the reaction field is determined by the solution of the SCF equations (i.e., by the ground state density) and interacts with, but is not changed by, the excited state density. The PCM-TDDFT equations (7) can be transformed into a non-Hermitian eigenvalue problem of half the dimension which involves the diagonalization of the matrix²³

$$[(\mathbf{A} - \mathbf{B})(\mathbf{A} + \mathbf{B})]_{ai\sigma, bj\sigma'}, \quad (13)$$

to find its eigenvalues, which correspond to the square of the excitation energies ω , and both its left, $\langle \mathbf{X} - \mathbf{Y} |$, and right $|\mathbf{X} + \mathbf{Y}\rangle$ eigenvectors, which form a biorthonormal set

$$\langle \mathbf{X}_m - \mathbf{Y}_m | \mathbf{X}_n + \mathbf{Y}_n \rangle = \delta_{mn}.$$

Note that, following the above transformation, the PCM contributions is only present in the $(\mathbf{A} + \mathbf{B})$ matrix. In this framework, the excitation energy for the n th state is computed as

$$\omega_n = \frac{1}{2} \langle \mathbf{X}_n + \mathbf{Y}_n | (\mathbf{A} + \mathbf{B}) | \mathbf{X}_n + \mathbf{Y}_n \rangle + \frac{1}{2} \langle \mathbf{X}_n - \mathbf{Y}_n | (\mathbf{A} - \mathbf{B}) | \mathbf{X}_n - \mathbf{Y}_n \rangle.$$

C. Analytical gradient of the excited state energy in the gas phase and in solution

The differentiation of the TDDFT excitation energy ω with respect to the generic nuclear coordinate ξ (Refs. 4 and 5) can be carried out along the same line as in Refs. 12 and 28. First, we note that the derivative expression

$$\begin{aligned} \omega_n^{\xi} = & \frac{1}{2} \langle \mathbf{X}_n + \mathbf{Y}_n | (\mathbf{A} + \mathbf{B})^{\xi} | \mathbf{X}_n + \mathbf{Y}_n \rangle \\ & + \frac{1}{2} \langle \mathbf{X}_n - \mathbf{Y}_n | (\mathbf{A} - \mathbf{B})^{\xi} | \mathbf{X}_n - \mathbf{Y}_n \rangle \end{aligned} \quad (14)$$

does not involve the derivatives of the excitation amplitudes [i.e., the left and right eigenvectors of Eq. (13)] because they have been variationally determined, but it does require the knowledge of the change in the elements of Fock matrix in the MO basis $F_{pq\sigma}^{\xi}$, which in turn requires the knowledge of the MO coefficients derivatives, which are the solution of the couple perturbed Kohn-Sham equations (CPKS). It is well known, however, that there is no need to solve the CPKS equations for each perturbation, but rather only for one degree of freedom, to find the so called Z vector²⁶ (or relaxed density), which represents the orbital relaxation contribution to the one-particle density matrices (1PDM) involved in all post-SCF gradient expressions.

Using a notation similar to that of Ref. 5, we define two contractions of a nonsymmetric density matrix \mathbf{P} with the four-indexes portion of the $(\mathbf{A} + \mathbf{B})$ and $(\mathbf{A} - \mathbf{B})$ matrices into the two-electron integrals portion of a nonsymmetric Fock-like matrix,

$$\begin{aligned} G_{pq\sigma}^{+}[P_{rs}] = & \sum_{rs\sigma'} [2(pq\sigma|rs\sigma') + 2f_{pq\sigma, rs\sigma'}^{\text{xc}} + 2\mathcal{V}_{pq\sigma, rs\sigma'}^{\text{PCM}} \\ & - c_x\delta_{\sigma\sigma'}[(ps\sigma|rq\sigma) + (pr\sigma|sq\sigma)]] P_{rs\sigma'}, \end{aligned}$$

$$G_{pq\sigma}^{-}[P_{rs}] = \sum_{rs\sigma'} [c_x\delta_{\sigma\sigma'}[(ps\sigma|rq\sigma) - (pr\sigma|sq\sigma)]] P_{rs\sigma'},$$

where the indexes on the argument matrix can be used to limit the range of the summation, e.g., $G_{ab\sigma}^{+}[P_{ij}]$ is the virtual-virtual block of the contraction of the occupied-occupied block of \mathbf{P} .

The quantities defined above could be computed in the MO basis, but in the actual implementation three steps are involved: (i) the density matrix to be contracted is transformed to the AO basis and the appropriate symmetric/antisymmetric component or spin combination is formed; (ii) the contraction is performed in a direct fashion with the AO two-electron integrals (or their suitable Raffennetti combinations²⁷); and (iii) the final Fock-like matrix is post-processed and back-transformed to the MO basis.

Using the above definitions it is possible to generalize the notation of Ref. 28 and write the Z-vector equation as

$$G_{ai\sigma}^{+}[P_{bj}^{\Delta}] + \delta_{ab}\delta_{ij}\delta_{\sigma\sigma'}(\epsilon_{a\sigma} - \epsilon_{i\sigma})P_{ai\sigma}^{\Delta} = L_{ai\sigma}, \quad (15)$$

where $L_{ai\sigma}$ is the TDDFT Lagrangian

$$\begin{aligned}
L_{ai\sigma} &= C1_{ai\sigma} - C2_{ai\sigma} + G_{ai\sigma}^+[P_{kl}^\Delta] + G_{ai\sigma}^+[P_{bc}^\Delta], \\
C1_{ai\sigma} &= \sum_b (X+Y)_{bi\sigma} G_{ba\sigma}^+ [(X+Y)_{rs}] \\
&\quad + \sum_b (X-Y)_{bi\sigma} G_{ba\sigma}^- [(X-Y)_{rs}] \\
&\quad + \sum_b (X+Y)_{bi\sigma} G_{ba\sigma}^{xc} [(X+Y)_{rs}], \\
C2_{ai\sigma} &= \sum_j (X+Y)_{aj\sigma} G_{ij\sigma}^+ [(X+Y)_{rs}] \\
&\quad + \sum_j (X-Y)_{aj\sigma} G_{ij\sigma}^- [(X-Y)_{rs}].
\end{aligned} \quad (16)$$

Note that the Lagrangian depends on the occupied-occupied and virtual-virtual blocks of the \mathbf{P}^Δ matrix which are already available from the diagonalization of (13) and are

$$\begin{aligned}
P_{ij\sigma}^\Delta &= -\frac{1}{2} \sum_a [(X+Y)_{ia\sigma} (X+Y)_{ja\sigma} \\
&\quad + (X-Y)_{ia\sigma} (X-Y)_{ja\sigma}], \\
P_{ab\sigma}^\Delta &= +\frac{1}{2} \sum_i [(X+Y)_{ia\sigma} (X+Y)_{ib\sigma} \\
&\quad + (X-Y)_{ia\sigma} (X-Y)_{ib\sigma}],
\end{aligned}$$

while the occupied-virtual block is the unknown in Eq. (15). The Lagrangian (16) includes the exchange-correlation term $G_{pq\sigma}^{xc}$ which involves the third derivative of E^{xc} and whose detailed expression is given in the Appendix. The current implementation also allows for “frozen core” calculations²⁹ where the range of excitations involved in the construction of the matrix (13) is limited only to a portion of the occupied and virtual MOs.

Using the definitions introduced in Secs. II A and II B, Eq. (14) can be transformed into its final form which is conveniently expressed in the AO basis as

$$\begin{aligned}
\omega^\xi &= \sum_{\mu\nu\sigma} h_{\mu\nu}^\xi P_{\mu\nu\sigma}^\Delta + \sum_{\mu\nu\sigma} S_{\mu\nu}^\xi W_{\mu\nu\sigma} \\
&\quad + \sum_{\mu\nu\kappa\lambda\sigma\sigma'} (\mu\nu|\kappa\lambda)^\xi \Gamma_{\mu\nu\sigma,\kappa\lambda\sigma'} + \omega^{xc,\xi} + \omega^{PCM,\xi}, \quad (17)
\end{aligned}$$

where we used μ, ν, \dots to indicate the atomic basis functions. We already defined \mathbf{P}^Δ which is the change in the 1PDM between the ground state and the excited state (including orbital relaxation effects) and $(\mathbf{X}+\mathbf{Y})$ which is the transition density [i.e., the right eigenvectors of matrix (13)]. The two-particle density matrix (2PDM) $\Gamma_{\mu\nu\sigma,\kappa\lambda\sigma'}$ collects all the contributions that multiply the integrals first derivatives $(\mu\nu|\kappa\lambda)^\xi$ and its expression is given in Ref. 5, while $h_{\mu\nu}^\xi$ and $S_{\mu\nu}^\xi$ are the derivatives of the one-electron Hamiltonian and the overlap matrix, respectively.

Equation (17) also includes two exchange-correlation contributions,

$$\begin{aligned}
\omega^{xc,\xi} &= \sum_{\mu\nu\sigma} V_{\mu\nu\sigma}^{xc(\xi)} P_{\mu\nu\sigma}^\Delta + \sum_{\mu\nu\kappa\lambda\sigma\sigma'} f_{\mu\nu\sigma,\kappa\lambda\sigma'}^{xc(\xi)} \\
&\quad \times (X+Y)_{\mu\nu\sigma} (X+Y)_{\kappa\lambda\sigma'},
\end{aligned}$$

where we have introduced the superscript (ξ) to label quantities involving only atomic basis functions derivatives. The first of the two XC contributions is common to all “post-Kohn-Sham” gradients as it depends on the change in the 1PDM, while the second one is specific to the TDDFT gradient as it involves the derivative of the XC matrix element $f_{\mu\nu\sigma,\kappa\lambda\sigma'}^{xc}$ in Eqs. (9) and (10). The form of these exchange-correlation terms, together with details on their evaluation, is given in the Appendix. The expression of the energy-weighted density matrix $W_{\mu\nu\sigma}$ is more easily given in the MO basis^{5,12,28}

$$\begin{aligned}
W_{ij\sigma} &= -P_{ij\sigma}^\Delta \epsilon_{i\sigma} - S1_{ij\sigma} - G_{ij\sigma}^+[P_{pq}^\Delta], \\
W_{ai\sigma} &= -C2_{ai\sigma} - P_{ai\sigma}^\Delta \epsilon_{i\sigma}, \\
W_{ab\sigma} &= P_{ab\sigma}^\Delta \epsilon_{a\sigma} - S2_{ab\sigma},
\end{aligned}$$

where

$$\begin{aligned}
S1_{ij\sigma} &= \frac{1}{2} \sum_a (X+Y)_{ia\sigma} G_{aj\sigma}^+ [(X+Y)_{rs}] \\
&\quad + \frac{1}{2} \sum_a (X-Y)_{ia\sigma} G_{aj\sigma}^- [(X-Y)_{rs}] \\
&\quad + \frac{1}{2} \sum_a (X+Y)_{ia\sigma} G_{aj\sigma}^{xc} [(X+Y)_{rs}], \\
S2_{ab\sigma} &= \frac{1}{2} \sum_i (X+Y)_{ia\sigma} G_{bi\sigma}^+ [(X+Y)_{rs}] \\
&\quad + \frac{1}{2} \sum_i (X-Y)_{ia\sigma} G_{bi\sigma}^- [(X-Y)_{rs}].
\end{aligned}$$

The gradient of the excitation energy includes two explicit PCM contributions, but the solvent reaction field also implicitly affects Eq. (17) through \mathbf{P}^Δ and \mathbf{W} ,

$$\begin{aligned}
\omega^{PCM,\xi} &= \sum_{\mu\nu\sigma} V_{\mu\nu\sigma}^{PCM(\xi)} P_{\mu\nu\sigma}^\Delta \\
&\quad + \sum_{\mu\nu\kappa\lambda\sigma\sigma'} V_{\mu\nu\sigma,\kappa\lambda\sigma'}^{PCM(\xi)} (X+Y)_{\mu\nu\sigma} (X+Y)_{\kappa\lambda\sigma'}.
\end{aligned}$$

The first explicit PCM contribution is common to all post-SCF gradients and involves the change in the 1PDM due to the specific post-SCF procedure,^{12,30}

$$\begin{aligned}
\sum_{\mu\nu\sigma} V_{\mu\nu\sigma}^{PCM(\xi)} P_{\mu\nu\sigma}^\Delta &= \sum_{\mu\nu\sigma} P_{\mu\nu\sigma}^\Delta \left[\sum_k V_{\mu\nu,k}^E q_k^w \right]^{(\xi)} \\
&= \sum_k V_k^{E,\Delta(\xi)} q_k^w + \sum_{kl} V_k^{E,\Delta} Q_{kl}^s V_l^{(\xi)} \\
&\quad + \sum_{kl} V_k^{E,\Delta} Q_{kl}^{s,\xi} V_l, \quad (18)
\end{aligned}$$

where we have used Eq. (6). In Eq. (18), $V_k^{E,\Delta}$ is the change in the solute's electronic electrostatic potential at the tesserae corresponding to the change in the 1PDM,

$$V_k^{E,\Delta} = \sum_{\mu\nu\sigma} P_{\mu\nu\sigma}^{\Delta} V_{\mu\nu,k}^E.$$

The second explicit PCM contribution to Eq. (17) is specific to the linear response theory and arises from the derivative of the reaction field matrix element $V_{\mu\nu\sigma,\kappa\lambda\sigma'}^{\text{PCM}}$ in the $(\mathbf{A}+\mathbf{B})$ matrix,

$$\begin{aligned} & \sum_{\mu\nu\kappa\lambda\sigma\sigma'} V_{\mu\nu\sigma,\kappa\lambda\sigma'}^{\text{PCM}(\xi)} (X+Y)_{\mu\nu\sigma} (X+Y)_{\kappa\lambda\sigma'} \\ &= 2 \sum_k V_k^{E,(X+Y)(\xi)} [q_k^w]^{E,(X+Y)} + \sum_{kl} V_k^{E,(X+Y)} Q_{kl}^{s,\xi} V_l^{E,(X+Y)}, \end{aligned} \quad (19)$$

where $V_k^{E,(X+Y)}$ and $[q_k^w]^{E,(X+Y)}$ are the contributions to the solute's electronic electrostatic potential and the polarization weights related to the transition density $(\mathbf{X}+\mathbf{Y})$,

$$V_k^{E,(X+Y)} = \sum_{\mu\nu\sigma} (X+Y)_{\mu\nu\sigma} V_{\mu\nu,k}^E,$$

$$[q_k^w]^{E,(X+Y)} = \sum_l Q_{kl}^s V_l^{E,(X+Y)}.$$

Note that, in the above expressions (18) and (19) the derivative of the electronic electrostatic potential are taken while keeping the MOs coefficients and the TDDFT amplitudes at their variationally determined values [hence the superscript in parentheses (ξ)]. However, since the positions of the tesserae \mathbf{s}_k ultimately depend on the nuclear coordinates, the (ξ) derivative as actually two terms

$$\begin{aligned} V_{\mu\nu}^{E(\xi)} = & - \int (\chi_{\mu}^*(\mathbf{r}) \chi_{\nu}(\mathbf{r}))^{\xi} \frac{1}{|\mathbf{r} - \mathbf{s}_k|} d\mathbf{r} \\ & - \frac{\partial \mathbf{s}_k}{\partial \xi} \cdot \left[- \int \chi_{\mu}^*(\mathbf{r}) \chi_{\nu}(\mathbf{r}) \frac{(\mathbf{r} - \mathbf{s}_k)}{|\mathbf{r} - \mathbf{s}_k|^3} d\mathbf{r} \right], \end{aligned}$$

where the latter term involves the geometrical derivatives of the cavity³¹ and the solute's electronic electric field at the tesserae. The quantities in Eqs. (18) and (19) involving the derivative of the \mathbf{Q} matrix can be calculated using different approaches. In the present implementation, the approach formulated by Cossi *et al.* has been used.²²

Equation (17) can be finally summed to the standard DFT contribution to give the expression for the total free energy gradient of each state in the presence of the solvent,

$$G^{\text{TDDFT},\xi} = G_{gs}^{\text{DFT},\xi} + \omega^{\xi}.$$

For the description of the ground state DFT gradient contribution $G_{gs}^{\text{DFT},\xi}$, the reader is referred to the original papers on the formulation of efficient analytical free energy gradients within the PCM scheme.²²

D. The relaxed density and the first order properties

The solution of the Z-vector equation (15) as well as the knowledge of eigenvectors $(\mathbf{X}+\mathbf{Y})_n$ and $(\mathbf{X}-\mathbf{Y})_n$ allows one to calculate the change \mathbf{P}_n^{Δ} in the one-particle density matrix between the ground and the excited state, for each excited state n .

The knowledge of \mathbf{P}^{Δ} is all it is required to evaluate the changes upon excitation of the first order properties. Among them, the most common example is the dipole moment which now becomes a difference between the excited and the ground state,

$$\Delta\mu_A = \text{tr} \mathbf{P}^{\Delta} \mathbf{m}_A, \quad A = x, y, z,$$

where \mathbf{m}_A is the dipole integrals matrix.

In the same way we can perform a population analysis of \mathbf{P}^{Δ} and thus obtain information on the charge redistribution and the change in bond order induced by an electronic excitation.

The inclusion of solvent effects enriches this kind of analysis. In fact, by tuning the value of the solvent dielectric permittivity ϵ , which is included in the expression of the \mathbf{Q} matrix, we can describe the changes in the excited state charge density when passing from the Franck-Condon region of the solvent coordinate (i.e., the nonequilibrium) to a completely relaxed solvent. This is done by changing the value of ϵ used to compute the polarization weights in Eqs. (6), (18), and (19) from the optical value ϵ_{∞} (namely, the square of the refractive index) to the static bulk value ϵ_0 . Effects of these changes can be significant for polar solvent for which $\epsilon_{\infty} \ll \epsilon_0$.

III. ENERGIES, STRUCTURES, AND PROPERTIES OF PNA AND DMABN EXCITED STATES

In this section, we present two case studies of the excited state properties and geometries of two molecules which show large solvent effects on both the energy and the structure of their lowest singlet excited states. In particular, the selected molecules, PNA and DMABN, are well-known examples of systems with excited states characterized by an intramolecular charge transfer and thus extremely sensitive to the presence of a stabilizing polar solvent. It is well known that the TDDFT tends to underestimate the charge-transfer excitation energies considerably due to spurious self-interaction.³² It is, however, also known that this error is reduced when hybrid functionals are used. The focus of the present work is on excited-state properties such as the structures which are generally much less affected by the self-interaction error than excitation energies. Nevertheless, in order to ensure a reasonable overall accuracy for our results, the hybrid B3LYP functional has been used, together with a triple-zeta basis set, namely, 6-311G(*d,p*). For both molecules the analysis of the excited states is limited to valence states, for which the use of larger basis sets including diffuse functions should not be necessary. However, in order to address this issue, we have repeated all the calculations on PNA using the 6-311+G(*d,p*) basis set and the results

obtained in this way (*vide infra*) have not shown significant differences with respect to the ones obtained using the smaller basis set. Thus only the 6-311G(*d,p*) has been used in the calculations carried out on DMABN.

In addition to the two applications presented in this section, papers dealing with the study of excited state PES by means of TDDFT in the gas phase³³ and including solvent effects³⁴ recently appeared in the literature.

In PCM calculations, the IEFPCM method⁷ has been used and the solute cavity has been built starting from a set of interlocking spheres centered on selected atoms and the scaled van der Waals radii have been used. For both systems the spheres have been centered on all atoms but the aromatic hydrogens which have been included in the sphere centered in the nearest carbon atom. Namely, we obtain 12 spheres for PNA and 11 spheres for DMABN with radii set to $R_C=2.04$ Å, $R_{CH}=2.28$, $R_N=1.92$, $R_O=1.824$, and $R_{H(N)}=1.44$. Two solvents have been chosen, an apolar and a polar one, namely, cyclohexane (with permittivity $\epsilon_0=2.02$ and $\epsilon_\infty=2.02$) and acetonitrile (with permittivity $\epsilon_0=36.64$ and $\epsilon_\infty=1.8060$).

All the calculations have been performed using a development version of the GAUSSIAN code³⁵ which includes the TDDFT gradient implemented as described in Sec. II C.

A. PNA

The PNA represents one of the simplest compounds showing intermolecular charge transfer (ICT) from $-\text{NH}_2$ to $-\text{NO}_2$, and therefore serves as an important model for theoretical^{36–38} and experimental^{39–44} studies.

The PNA has an intense absorption band in the near ultraviolet to visible spectral region which strongly depends on the solvent polarity and thus indicates a large increase of the molecular dipole moment upon optical excitation. In the gas phase this band peaks at 4.24 eV (Ref. 41) whereas it is redshifted by 0.39 eV in cyclohexane and by 0.83 eV in acetonitrile.⁴⁴ In the excited PNA molecules, both the strong donor and the strong acceptor groups may modify their conformation, leading to an increased intramolecular charge separation. The twisting of the nitro group relative to the central benzene moiety was first considered in Ref. 42 where it was shown that in the excited state the dipole moment is larger when the $-\text{NO}_2$ is twisted compared to the coplanar conformation and that the twisted state is stabilized in highly polar solvents.

More recently, transient absorption spectra in acetonitrile and water have been measured by Kovalenko *et al.*⁴⁴ in a range 300–700 nm with 30 fs resolution, allowing for the observation of the complete spectral evolution. According to these studies, the relaxation of the PNA molecule after photoexcitation is initiated by the twist of $-\text{NO}_2$ to a new equilibrium position. More specifically, the relaxation involves several stages corresponding to different processes. The fastest process develops on a 10 fs time scale and corresponds to intramolecular vibrational relaxation of the high frequency modes. The next process, on a 100 fs time scale, corresponds to solvent relaxation and it is observed as the dynamic Stokes shift of the stimulated emission band. Intramolecular

TABLE I. TDDFT and experimental ICT excitation energies (eV) of pNA in gas phase and in solution. For solvated systems we also report calculated and observed gas-to-solution shifts. **The experimental energies correspond to absorption spectral maxima.**

	TDDFT	Exp.
Vacuum	4.07	4.24
Cyclohexane	3.82	3.85
(Shift)	0.25	0.39
Acetonitrile	3.63	3.41
(Shift)	0.44	0.83

charge transfer and internal conversion are accessed by the twisting of $-\text{NO}_2$ as it is driven to the new equilibrium position. This happens roughly between 100 fs and 1 ps and it is recognized in the simultaneous decay of the excited state absorption and the simulated emission band.

Following these observations we have applied the TD-DFT approach described in the previous section to calculate the ICT transition energies and relaxed geometries of the PNA in cyclohexane and acetonitrile. In addition, we have also calculated the dipole moment and the (natural bond orbitals) (NBO) charges⁴⁵ at the geometry of the ground and of the excited state in order to describe the changes from the Franck-Condon to the relaxed excited state. Moreover, in the case of the polar solvent we have compared equilibrium and nonequilibrium solvation to study the effect of the solvent reorganization on these properties.

In Table I we report the calculated and experimental vertical excitation energies in the gas phase and in the two solvents. The calculated values refer to the ground state (GS) geometries [obtained at the B3LYP/6-311G(*d,p*) level] and in the case of acetonitrile to nonequilibrium solvation.

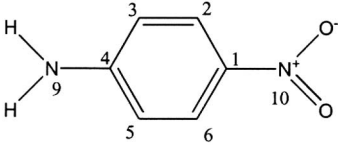
The calculated values correctly reproduce the experimental trend from gas phase to cyclohexane and acetonitrile. More quantitatively, we found a redshift of 0.25 eV in cyclohexane and 0.44 eV in acetonitrile. These results indicate an underestimation of the solvent effect when compared to the experimental shifts of 0.39 and 0.83 eV. A probable reason for this underestimation (or at least for a part of it) is related to the DFT description which amplifies the solvent polarization effects on GS while it cannot stabilize enough the ICT excited state (see below for further details). As a result the redshift calculated is smaller than the observed one.

The main geometrical parameters for the GS and the CT state in gas phase and in the two solvents are reported in Tables II and III, respectively.

Both in gas phase and in solution, the molecule is essentially planar; only $-\text{NH}_2$ is slightly wagged (but not twisted) as shown by the wagging dihedral angle $\varphi_w(\text{HN}_9\text{C}_4\text{C}_3)$: such a wagging decreases in more polar solvents. In all cases, the calculations of the Hessian were performed and confirmed that the geometries really correspond to a minimum.

The solvent effects show a clear trend. As the polarity of the solvent increases (from gas phase to cyclohexane to acetonitrile), the pattern of the bond lengths changes, the C_4C_3 bond length increases, while the C_1N_{10} , C_3C_2 , and C_4N_9

TABLE II. Main geometrical parameters for the GS state in gas and in the two solvents.



	Vacuum	Cyclohexane	Acetonitrile
$R(C_4N_9)$	1.376	1.370	1.357
$R(C_4C_3)$	1.409	1.412	1.417
$R(C_3C_2)$	1.382	1.381	1.378
$R(C_2C_1)$	1.394	1.396	1.400
$R(C_1N_{10})$	1.462	1.456	1.442
$R(N_{10}O)$	1.227	1.230	1.235
$\varphi_w(HN_9C_4C_3)$	19.2	17.2	11.2
$\varphi_t(ON_{10}C_1C_2)$	0.0	0.0	0.0

bond lengths decrease, thus amplifying their respective single and double bond characters. Such a behavior is easily explained using the common picture of two molecular resonance structures, the neutral and the zwitterionic, and observing that in more polar solvents the weight of the zwitterionic structure is increased and accounts for the changes in the geometry.

Next, we consider the CT excited state. The main geometrical parameters calculated both in gas and in solution are reported in Table III.

The first remark is that both in gas phase and in solution the minimum of the ICT state is a $-NO_2$ twisted structure; we note, however, that this twisting also involves a wagging of the oxygen atoms thus leading to a net dihedral angle of about 70° . Due to this deformation, the oxygen atoms are closer to a side of the aromatic moiety (here the C_2C_3 side) and thus the bond lengths are no longer symmetric. We note that the solvent effects for the ICT state are generally small, the main differences being in the C_4N_9 and the C_1N_{10} bond lengths.

Both for the isolated and solvated systems, the main changes from GS to ICT state are found in the $N_{10}O$ bond length which in the ICT state becomes significantly longer

and in the C_4N_9 bond which becomes shorter. In gas phase we also observe a significant decrease in the C_1N_{10} bond length.

Few among the many theoretical studies of PNA explicitly consider excited state molecular geometries. Among them, we cite here the work of Kovalenko *et al.*,⁴⁴ who performed semiempirical SAM1 calculations on the excited state nuclear dynamics of PNA in gas phase and in water (using the COSMO mode⁴⁶) and a successive study by Moran *et al.*³⁸ using an excited state molecular dynamics (MD) approach to calculate both ground and excited electronic state equilibrium geometries. In the latter study the simulations were performed by combining the AM1 semiempirical Hamiltonian with the CEO method¹⁴ and solvent effects were incorporated using the Onsager formulation of the self-consistent reaction field. In both studies the equilibrium geometry of the CT excited state was found to have a greater zwitterionic character compared to that of the ground state which resulted in corresponding changes of the bond-length alternation. The only exception with respect to this two-state model was given by the increase of the C_1N_{10} in acetonitrile (but not in gas phase or in cyclohexane) and the twisting of the NO_2 group in acetonitrile (ca. 25° in the AM1 study and 90° in the SAM1 study).

In the study by Moran *et al.*,³⁸ a comparison with experiments was also presented using the resonance Raman (RR) data measured by Moran and Kelley.⁴⁰ We note, however, that the use of the RR technique is to get information about the geometry changes from the ground to the excited state is based on models that involve drastic assumptions which necessarily weaken the reliability of the results. This technique, in fact, does not allow a direct determination of absolute geometry changes since the measured intensities depend only on the magnitudes and not on the signs of the dimensionless mode displacements. The determination of respective signs requires the selection of the most probable signs combination among the $2N$ possibilities (N is the number of Raman active normal modes). The resulting values thus depend on the requirements imposed by the experimentalists. In particular, in Moran and Kelley's study the selection was made by requiring that the direction of the geometry change is expected for a transition to a more zwitterionic state. More specifically,

TABLE III. TDDFT optimized geometrical parameters for the ICT state in gas phase and in the two solvents. The values in parentheses refer to the calculations including diffuse basis functions on the heavy atoms.

	Vacuum	Cyclohexane	Acetonitrile
$R(C_4N_9)$	1.351 (1.352)	1.344 (1.344)	1.333 (1.331)
$R(C_4C_{3/5})$	1.424/1.423 (1.425/1.423)	1.427/1.425 (1.428/1.426)	1.432/1.430 (1.433/1.433)
$R(C_{3/5}C_{2/6})$	1.367/1.374 (1.368/1.374)	1.367/1.373 (1.367/1.373)	1.367/1.372 (1.367/1.371)
$R(C_{2/6}C_1)$	1.416/1.408 (1.415/1.408)	1.414/1.408 (1.413/1.408)	1.414/1.408 (1.414/1.408)
$R(C_1N_{10})$	1.419 (1.422)	1.428 (1.430)	1.429 (1.431)
$R(N_{10}O)$	1.304 (1.303)	1.305 (1.305)	1.307 (1.307)
$\varphi_w(HN_9C_4C_3)$	0.0	0.0	0.0
$\varphi_t(ON_{10}C_1C_2)$	71.1 (71.6)	71.8 (72.1)	72.6 (73.7)

TABLE IV. TDDFT and experimental ground state and a Franck-Condon ICT dipole moments μ (in Debye) of pNA in gas phase and in solution. Values in parentheses refer to the previous CASSCF calculations (Ref. 37).

	GS		ICT	
	Calc.	Exp.	Calc.	Exp.
Vacuum	7.2 (6.1)	6.2	12.4 (17.2)	15.3 \pm 1
Cyclohexane	8.3 (6.9)	7.4 ^a	14.0 (19.4)	18 \pm 1 ^a
Acetonitrile	10.5 (7.9)		14.2 (19.7)	

^aIn dioxane (Ref. 43)

they required that the NO bonds lengthens, the C₄N₉ bond shortens, and the phenyl C₂C₃ bonds also shorten. Indeed, all these requirements are confirmed by our calculations even if the agreement is not quantitative. The discrepancies can be due to different reasons but it is worth noting that, as the RR intensities are sensitive mainly to the excited state surface near the Franck-Condon region with respect to both the internal and solvent modes, it is most appropriate to use the description of the excited state at the ground state equilibrium value of the solvent coordinates while our calculations have been done assuming a completely relaxed solvent. Indeed, our model is appropriate for the prediction of the equilibrium geometry in the excited states, while a nonequilibrium treatment would have been more suited for the comparison with the RR experiments. In addition we note that to extract the “experimental” displacements a preliminary knowledge of the GS normal modes from DFT calculations on the isolated system was exploited.

Unfortunately, the resonance Raman experiments on PNA cannot detect the low frequency modes corresponding to the NH₂ wagging and the NO₂ twisting and thus no confirmation of the twisted structure can be obtained in this way.

We conclude the analysis of the solvent effects on the CT state of PNA by considering the dipole moments and the NBO charges calculated with the relaxed density matrix (see Sec. II D).

In order to allow for a comparison with the experimental data we first consider the Franck-Condon ICT states, i.e., we calculate the dipole moments of the excited state by keeping the geometry frozen in the ground state. The results are reported in Table IV.

As previously done for the geometry displacements also in the case of dipole moments we have to add some comments on the experimental data. The latter are reported in Table IV for gas phase and they have been extracted from the measurements in dioxane solution by applying the Onsager reaction field model to eliminate the solvent effect.⁴³ In contrast, the cyclohexane experimental dipole moments have been obtained from those reported in Ref. 43 reincluding the proper reaction field factors [see Eqs. (3)–(5) of the same reference for the expressions used]. Given these facts, we note that the observed solvent induced changes on both the ground and excited state dipole moments are quantitatively reproduced by the calculations.

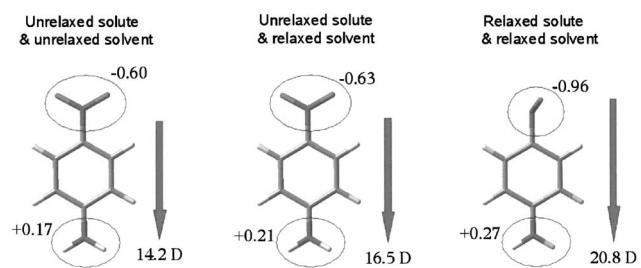


FIG. 1. Graphical representation of the change in the NBO charges and the dipole moment of the PNA excited state not allowing (left) or allowing for solvent (center) and solute geometry (right) relaxation. Charges are in a.u. and dipole moments in Debye.

Another interesting test for the accuracy of our results is the comparison with a previous IEFPCM-CASSCF calculation³⁷ (for a direct comparison, these data are reported in Table IV). In that case the calculated solvent induced changes in the dipole moments were +0.8 D in the apolar solvent and +1.8 D in the polar solvent for GS, while they were +2.2 D and +2.5 D for ICT state. When these data are compared with the TDDFT results reported in Table IV it is apparent that the DFT calculations amplify the solvent polarization effects on GS (for which both the absolute values and the gas-to-solvent shifts are larger CASSCF level) while they give a less polarized and polarizable ICT state.

As we have noted the data reported in Table IV refer to the Franck-Condon CT states; it thus becomes interesting to analyze the effects of both the solute and the solvent relaxation. For the apolar cyclohexane, solvent relaxation effects are null whereas they are large for the polar acetonitrile, as shown in Fig. 1 in where we show a graphical representation of the evolution of the dipole moment and of the NBO charges of the ICT state of PNA in acetonitrile when we allow for both the solvent and solute geometry relaxation.

As shown by the relative changes in both the NBO charges and the dipole moment, the solvent relaxation induces an increase of 10% in the charge transfer and of 16% in the dipole moment whereas the effect of the twisting (and of the related changes in the order geometrical parameters) gives a further 46% charge transfer and a further 26% dipole moment increase.

B. DMABN

The DMABN represents the paradigm of anomalous emissive behavior or dual fluorescence which consists in an additional emission (*A* band) redshifted with respect to the “normal” emission band (*B* band). Generally, the *A* band is ascribed to an ICT state, whose formation should be favored in the polar solvents as compared to the less polar “locally excited” (LE) state which gives rise to the *B* band.

Since the first observation of dual fluorescence in DMABN by Lippert *et al.* in 1959,⁴⁷ a number of other compounds exhibiting dual fluorescence were discovered. However, DMABN still remains one of the most studied examples, and not only for historical reasons. The relatively small dimensions, now easily tractable with accurate compu-

tational tools, and the numerous experimental data available for comparison have made DMABN a challenging test for different *ab initio* methods, and, in fact, many calculations, at various levels, have been performed, in particular, in the past few years.⁴⁸

Despite these numerous studies, the mechanism of the ICT in DMABN is still a controversial matter. Among the proposed mechanisms, we cite here the twisted intramolecular charge transfer (TICT) model by Rotkiewicz *et al.*⁴⁹ According to the TICT model the newly formed excited state yields towards another minimum on its potential energy surface by twisting the dialkylamino group from a planar (or nearly planar) to a perpendicular position with respect to the benzonitrile ring. The twisting is accompanied by an intramolecular charge transfer from the donor (the amino group) to the acceptor moiety (the benzonitrile group). The resulting excited state, characterized by a large intramolecular charge separation and an increased dipole moment, can be stabilized in the polar solvents, thus leading to the observed “anomalous” second fluorescence band. On the other hand, the “standard” *B* band, is assigned to the less polar LE state, where no twisting has occurred.

Besides the TICT, other models have been proposed in which no twisting is required to lead to the CT state; as an example, we cite here the so-called planar ICT (PICT) model advocated by Zachariasse *et al.*⁵⁰ This model assumes the presence of a quinoidal ICT state with a slightly pyramidalized Me₂N group and the ICT reaction coordinate involves the Me₂N out-of-plane angle and the quinoidal ring deformation.

An important contribution towards the settlement of this open controversy should come from the QM studies in which both the energetics and the geometries of the relevant states can be determined along the reaction coordinate. However, this has not been the case until very recently. In fact, the implementations of analytical derivatives for the excited states correlated methods were not available, or the cost was still prohibitive or they were limited to the gas-phase systems. To the best of our knowledge, the only example of QM geometry optimizations of the LE and ICT states including solvent effects is a study carried out by some of the present authors¹² at the CIS level using PCM. In a successive study⁵¹ the same authors also used a multireference perturbed CI approach still with PCM but, due to the lack of analytical derivatives, geometry optimization was not performed. The energies of the excited states were simply plotted against the twisting angle while keeping the rest of the geometry frozen in the ground state optimized minimum. The twisting angle was varied from 0° to 90°. The main result of this study was that the twisting curves of the various states in the presence of a polar solvent are significantly different from the ones obtained in the gas phase. In fact, the highly polar ICT excited state can be stabilized much more effectively than the less polar LE state, thus leading to an inversion of their relative energies even at a nontwisted geometry. This behavior was found only once before, in the calculations by Gedeck and Schneider,⁵² all other previous studies including solvent

effects, in fact, showed the preferential stabilization of the ICT state with respect to LE but they were only limited to a few specific conformations and did not explore the whole energy profiles. The second important finding in the MRCI study was the large stabilization of the ICT state at the twisted geometry which turned out to be the global minimum on the curve; the twisted conformation lied 19.5 kcal/mol below the planar one, and the thermodynamic equilibrium of the charge-transfer reaction was therefore almost totally shifted towards the twisted conformation.

In the present work, we reconsidered the problem of photoinduced ICT in DMABN by means of the time-dependent density functional methods. Recently a TDDFT study on excited states structures and properties have appeared but is still limited to isolated DMABN.³³ The two lowest singlet excited states were characterized using TDDFT in gas phase, and their energies were found to cross at a twisting angle near 50°. In particular, the most stable excited state at the nontwisted geometry (the LE state) shows a very small dependence on the twisting angle, while the second one (the ICT state) shows a strong dependence with a minimum at 90°. This leads to the crossing of the corresponding energy curves. Here we repeated the LE and ICT TDDFT optimizations both in gas phase and in two solvents, the apolar cyclohexane and the polar acetonitrile (ACN) using the same B3LYP functional used in the reference gas-phase paper and a triple-zeta basis set, namely, 6-311G(*d,p*).

Before exploring the excited states potential energy surface, however, we have calculated the vertical excitations keeping the DMABN in the ground state optimized geometries in each solvent (and in gas phase). The results obtained for the first two excited states are reported in Table V. For the polar solvent (ACN) two sets of data are reported, one assuming a nonequilibrium response of the solvent and the other assuming a completely (equilibrated) response.

In Table V, the state having its major contribution from the highest occupied molecular orbital (HOMO) → lowest unoccupied molecular orbital (LUMO)+1 transition is the LE state while the one mainly described by a HOMO → LUMO transition is the ICT state. This is confirmed by the NBO charges on the donor/acceptor pair (NMe₂ and CN and groups) and it is also apparent from the graphical representation of the MOs involved (see Fig. 2).

In order to properly compare the PCM-TDDFT excitation energies reported in Table V with the experimental absorption spectra it is better to consider gas-to-solvent shifts instead of absolute energies; this for two simple reasons. The first is that the experimental data refer to absorption maxima while the calculated ones are vertical excitations and thus we can assume that the error we introduce by comparing these different values is smaller when the shifts are considered. The second, and more important reason is that absolute energies are largely affected by the intrinsic limitations of the QM method being used (here TDDFT) and thus the analysis of the solvent effects can be difficult due to the combination

TABLE V. Excitation energies (in eV), oscillator strengths (f), and NBO charges of DMABN in gas phase and in solution for the two lowest excited states. For all excitations we also report the major orbital changes contributing to the transition. For cyclohexane and for nonequilibrium acetonitrile the solvent shifts on the excitation energies are reported.

	VAC	CYC	ACN (neq)	ACN (eq)
ΔE	4.46	4.43 (−0.03) ^a	4.40 (−0.06) ^a	4.27
f	0.0311	0.0408	0.0356	0.8919
Main contr.	HOMO→LUMO+1	HOMO→LUMO+1	HOMO→LUMO+1	HOMO→LUMO
NBO(CN)	−0.033	−0.032	−0.062	−0.239
NBO(NMe ₂)	+0.177	+0.297	+0.333	+0.258
ΔE	4.71	4.54 (−0.17) ^b	4.44 (−0.27) ^b	4.36
f	0.5263	0.6699	0.6678	0.0620
Main contr.	HOMO→LUMO	HOMO→LUMO	HOMO→LUMO	HOMO→LUMO+1
NBO(CN)	−0.133	−0.176	−0.216	−0.058
NBO(NMe ₂)	+0.179	+0.211	+0.233	+0.351

^aThe experimental shift in cyclohexane is −0.15 eV while it cannot be measured in acetonitrile (Ref. 53).

^bThe experimental shift is −0.16 and −0.36 eV in cyclohexane and in acetonitrile, respectively (Ref. 53).

of physical and numerical issues. The experimental solvent induced shifts⁵³ of the LE and CT excitation energies are −0.15 and −0.16 eV in cyclohexane, respectively, while for ACN only the shift of the CT absorption can be observed (−0.36 eV). If we analyze the data reported in Table V we find that the TDDFT shifts are very accurate for the CT state: −0.17 eV in cyclohexane and −0.27 eV in ACN, which becomes −0.44 eV when we allow for the complete relaxation of the solvent response. The agreement is worse for the LE state for which the calculated −0.03 eV shift in cyclohexane is underestimated.

Another important comment is in order about the data reported in Table V. In ACN, if we allow for a complete solvent relaxation (equilibrium solvation) the order of the excited states is reverted even if the solute geometry is not relaxed. Indeed, the ICT state becomes the lowest state even at the GS geometry.

This important effect related to the solvent relaxation (or reorganization) has to be further examined by considering also the relaxation of the molecular geometry. We will assume that the same time evolution described for PNA, namely, an initial relaxation of the solvent at fixed geometry

followed by the twisting towards the new equilibrium position, is also valid for DMABN. Thus, we will use equilibrium solvation for the prediction of the excited state optimized geometry. The results of these calculations for the excited states planar and twisted conformation in both solvents are reported in Tables VI and VII. In Table VI the main geometrical parameters are shown for each state in both solvents whereas in Table VII energies and dipole moments are reported together with the corresponding ground state properties.

TABLE VI. Main geometrical parameters for the planar and twisted excited states in gas and in the two solvents. The values in parentheses are the percentage change with respect to the gas-phase parameters.

	VAC		CYC		ACN	
	planar		planar		planar	
$R_{CN(Me)}$	1.4110	(+2.67)	1.4093	(+2.86)	1.4030	1.4074
R_1	1.4070	(−0.64)	1.4073	(−0.76)	1.4092	1.4269
R_2	1.4353	(+3.80)	1.4367	(+3.96)	1.4383	1.3751
R_3	1.4076	(+0.32)	1.4069	(+0.18)	1.4069	1.4467
R_{CC}	1.4264	(−0.15)	1.4273	(+0.23)	1.4277	1.3957
R_{CN}	1.1577	(+0.09)	1.1576	(+0.02)	1.1580	1.1784
					(−0.07)	(+1.70)
	twisted		twisted		twisted	
$R_{CN(Me)}$	1.4426	(+4.98)	1.4381	(+4.96)	1.4312	(+4.85)
R_1	1.4216	(+0.38)	1.4214	(+0.24)	1.4218	(+0.06)
R_2	1.3691	(−1.00)	1.3692	(−0.91)	1.3695	(−0.82)
R_3	1.4408	(+2.69)	1.4420	(+2.69)	1.4447	(+2.71)
R_{CC}	1.4001	(−1.80)	1.3976	(−1.86)	1.3933	(−1.94)
R_{CN}	1.1683	(+1.00)	1.1705	(+1.13)	1.1741	(+1.31)

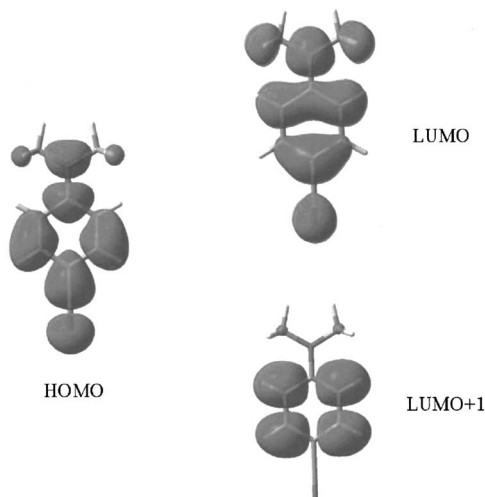


FIG. 2. Graphical representation of the HOMO, LUMO, and LUMO+1 for DMABN at the ground state geometry.

TABLE VII. Energies (in a.u.) and dipole moments (in Debye) of the optimized planar and twisted states in gas phase and in solution. Values in parentheses are the energy differences (in eV) with respect to the ground state in each phase.

	VAC		CYC		ACN	
	<i>E</i>	μ	<i>E</i>	μ	<i>E</i>	μ
GS	-458.579 060 4	7.772	-458.584 254	8.8142	-458.592 029 6	10.3365
LE	-458.422 000 3 (4.274)	10.536	-458.428 833 4 (4.229)	12.010	-458.439 257 3 (4.157)	14.057
ICT	-458.440 124 2 (4.134)	15.191
TICT	-458.451 741 5 (3.464)	15.682	-458.459 260 6 (3.401)	17.572	-458.470 438 4 (3.309)	20.361

In gas phase and in cyclohexane the nontwisted minimum corresponds to the LE state while the second excited singlet state (ICT) upon optimization relaxes into a minimum with a 90° twisted amino group conformation (TICT). On the contrary, in acetonitrile, the ICT state is the lowest state even at the nontwisted geometry (see also Table IV) and it corresponds to a minimum.

The nature of each state is confirmed by the differences in the main geometrical parameters. In fact, in the LE state we observe a significant increase in the R_2 and $R_{\text{CN(Me)}}$ bond lengths which is consistent with an increased quinoidal character of the structure, while the R_{CC} bond length does not change significantly. For the TICT state, besides the twisting of the amino group, we find a net increase of the R_{CN} and a corresponding decrease of the R_{CC} lengths accompanied by a significant increase of the R_3 and the $R_{\text{CN(Me)}}$ lengths. This is an expected consequence of the charge transfer from the donor (the amino group) to the acceptor moiety (the benzonitrile group). It is interesting to note that a similar behavior (with the exception of the twisting) is found for the planar ICT state in acetonitrile.

Next, we consider the energies and the dipole moments reported in Table VII. The inversion in the order of the vertical states found in ACN when an equilibrium solvent response is used (see Table V) is still present when we allow for geometry relaxation. However, the difference between the two nontwisted states is now reduced to about 0.5 kcal/mol with respect to the 2 kcal/mol found for the vertical states. These results are in perfect agreement with what was found in the previous MRCI study⁵¹ not only from a qualitative point of view but also quantitatively. In fact, the energy difference between the optimized planar and the twisted structures of the ICT state is 19.02 kcal/mol at TD-DFT level, whereas in the previous study (in which the structures were not completely relaxed as explained above) was 19.5 kcal/mol.

In the gas-phase TDDFT study of DMABN by Rapoport and Furche³³ the minimum energy paths (MEPs) for the ICT and LE states along the reaction coordinate were also presented as a result of a geometry optimization where all the internal degrees of freedom except the twisting angle were relaxed and the conservation of C_2 symmetry was

imposed. Significant results that study were the location of the intersection of the LE and ICT states at twisting angle $\vartheta=52^\circ$ and the small slope of the LE curve, which was found to be essentially flat. According to the authors, both observations imply that the LE-state minimum is metastable with respect to the ICT-state minimum at $\vartheta=90^\circ$. In the present paper, we have shown that this picture can be modified by the inclusion of solvent effects. In fact, in a polar solvent the preferential stabilization of the ICT state can lead to an intersection of the LE and ICT states even without relaxing the geometry but simply allowing for a complete solvent relaxation.

This result, already observed at the MRCI level, and here confirmed at the TDDFT level, is interesting as it provides a new way of looking at the dual fluorescence phenomenon and, hopefully, a step forward in the debate on the ICT mechanism.

IV. CONCLUSIONS

In this paper, we presented the theory and implementation of analytic derivatives of TDDFT excited states energies, both *in vacuo* and including solvent effects by means of the polarizable continuum model. Despite the increased complexity introduced by the solute-solvent interaction in the study of excited states energies and potential energy surfaces, TDDFT is confirmed as a powerful and useful tool, being both accurate and computationally affordable. In addition, the PCM-TDDFT approach offers in a very straightforward way the flexibility required to correctly describe both the nonequilibrium and equilibrium solvations. However, when used to model excited states in solution, TDDFT has limitations, common to all other linear response formalisms,¹³ and future work will better assess this issue and compare more thoroughly TDDFT with state specific wave function methods as already discussed in the Introduction. We also reported on the application of PCM-TDDFT to two case studies: p-nitroaniline (PNA) and 4-(dimethyl)aminobenzonitrile (DMABN). For both molecules PCM-TDDFT is shown to be successful in supporting the analysis of experimental data and providing useful insights for a better understanding of photophysical and photochemical pathways in solution.

APPENDIX: DETAILS ON THE EVALUATION OF THE EXCHANGE-CORRELATION TERMS

In this appendix, we establish a general framework for the evaluation of the exchange-correlation energy and its derivatives and we provide a more detailed description of the various terms involved in the excitation energy gradient, with respect to what can be found in Ref. 5. First, we express the exchange-correlation energy as

$$E^{\text{xc}} = \sum_g w_g F_g[\{z_I(\mathbf{P}, \dots)\}],$$

where w_g are the numerical quadrature weights and F_g are the functional values evaluated at the grid points. The functional itself depends on a set of variables $\{z_I\}$ which in turn depend either linearly or quadratically on a generic 1PDM \mathbf{P} . Currently, in our implementation we allow for the use of six variables linear in \mathbf{P} , namely, the density, the kinetic energy density, and the Laplacian of the density (both alpha and beta),

$$\rho_\sigma(\mathbf{P}) = \sum_{\mu\nu} P_{\mu\nu}^\sigma (\chi_\mu \chi_\nu),$$

$$\tau_\sigma(\mathbf{P}) = \sum_{\mu\nu} P_{\mu\nu}^\sigma (\nabla \chi_\mu \cdot \nabla \chi_\nu),$$

$$l_\sigma(\mathbf{P}) = \sum_{\mu\nu} P_{\mu\nu}^\sigma \nabla^2 (\chi_\mu \chi_\nu),$$

and three variables quadratically dependent on \mathbf{P}

$$\begin{aligned} \gamma_{\sigma\sigma'}(\mathbf{P}, \mathbf{Q}) &= \nabla \rho_\sigma(\mathbf{P}) \cdot \nabla \rho_{\sigma'}(\mathbf{Q}) \\ &= \left(\sum_{\mu\nu} P_{\mu\nu}^\sigma \nabla (\chi_\mu \chi_\nu) \right) \left(\sum_{\kappa\lambda} Q_{\kappa\lambda}^{\sigma'} \nabla (\chi_\kappa \chi_\lambda) \right). \end{aligned}$$

In the above definitions we used σ, σ' as spin labels and $\{\chi_\mu\}$ to indicate the atomic basis set.

We introduce now three new sets of quantities indicated as $u_I(\mathbf{Q})$, $u_{I,\mu\nu}$, and $v_{I,\mu\nu}$; their form is given in the following table for each of the z_I variable (ρ , τ , l , and γ), namely,

	ρ_σ	$\gamma_{\sigma\sigma'}$	$\gamma^{\sigma\sigma'}$	τ_σ	l_σ
$v_{I,\mu\nu}$	$(\chi_\mu \chi_\nu)$	$\nabla(\chi_\mu \chi_\nu)$	$\nabla(\chi_\mu \chi_\nu)$	$(\nabla \chi_\mu \cdot \nabla \chi_\nu)$	$\nabla^2(\chi_\mu \chi_\nu)$
$u_I(\mathbf{Q})$	1	$2 \nabla \rho_{\sigma'}(\mathbf{Q})$	$\nabla \rho_{\sigma'}(\mathbf{Q})$	1	1
$u_{I,\mu\nu}$	0	$2 \nabla(\chi_\mu \chi_\nu)$	$\nabla(\chi_\mu \chi_\nu)$	0	0

Using this formalism, the derivatives of the z_I variables with respect to the generic density matrix element $P_{\mu\nu}^\sigma$ become

$$\frac{\partial z_I(\mathbf{P}, \mathbf{Q})}{\partial P_{\mu\nu}^\sigma} = u_I(\mathbf{Q}) v_{I,\mu\nu},$$

whereas the exchange-correlation contribution to the $G_{\mu\nu\sigma}^+$ contraction in the AO basis can be written as

$$\begin{aligned} f_{\mu\nu\sigma, \kappa\lambda\sigma'}^{\text{xc}} &= \frac{\partial^2 E^{\text{xc}}}{\partial P_{\mu\nu}^\sigma \partial P_{\kappa\lambda}^{\sigma'}} \\ &= \sum_g w_g \sum_{IJ} \frac{\partial^2 F}{\partial z_I \partial z_J} \bigg|_g u_{J,g}(\mathbf{P}) v_{J,g,\mu\nu} u_{I,g}(\mathbf{P}) v_{I,g,\kappa\lambda} \\ &\quad + \sum_g w_g \sum_I \frac{\partial F}{\partial z_I} \bigg|_g u_{I,g,\kappa\lambda} v_{I,g,\mu\nu}. \end{aligned}$$

Its derivatives with respect to the MOs coefficients contribute to the Lagrangian in the following form:

$$\begin{aligned} G_{\mu\nu\sigma}^{\text{xc}} &= \frac{\partial}{\partial P_{\mu\nu}^\sigma} \left[\sum_{\kappa\lambda\sigma', \eta\omega\sigma''} f_{\kappa\lambda\sigma', \eta\omega\sigma''}^{\text{xc}} (X+Y)_{\kappa\lambda\sigma'} (X+Y)_{\eta\omega\sigma''} \right] \\ &= \frac{\partial}{\partial P_{\mu\nu}^\sigma} \left[\sum_g w_g \sum_{IJ} \frac{\partial^2 F}{\partial z_I \partial z_J} \bigg|_g u_J(\mathbf{P}) v_J(\mathbf{X}+\mathbf{Y}) u_I(\mathbf{P}) v_I(\mathbf{X}+\mathbf{Y}) + \sum_g w_g \sum_I \frac{\partial F}{\partial z_I} \bigg|_g u_I(\mathbf{X}+\mathbf{Y}) v_I(\mathbf{X}+\mathbf{Y}) \right] \\ &= \sum_g w_g \sum_{IJK} \frac{\partial^3 F}{\partial z_I \partial z_J \partial z_K} \bigg|_g u_K(\mathbf{P}) v_K(\mathbf{X}+\mathbf{Y}) u_J(\mathbf{P}) v_J(\mathbf{X}+\mathbf{Y}) u_I(\mathbf{P}) v_{I,\mu\nu} \\ &\quad + 2 \sum_g w_g \sum_{IJ} \frac{\partial^2 F}{\partial z_I \partial z_J} \bigg|_g u_J(\mathbf{P}) v_J(\mathbf{X}+\mathbf{Y}) u_{I,\mu\nu} v_I(\mathbf{X}+\mathbf{Y}) + \sum_g w_g \sum_{IJ} \frac{\partial^2 F}{\partial z_I \partial z_J} \bigg|_g u_J(\mathbf{X}+\mathbf{Y}) v_J(\mathbf{X}+\mathbf{Y}) u_I(\mathbf{P}) v_{I,\mu\nu}, \end{aligned}$$

where we omitted the obvious grid point index on some quantities.

On the other hand, the derivative with respect to the generic nuclear coordinate ξ , which does not involve any explicit derivatives of the MOs coefficients nor of the excitation amplitudes, can be written as

$$\begin{aligned}
f^{\text{xc}(\xi)} &= \frac{\partial}{\partial \xi} \left[\sum_{\kappa\lambda\sigma'\eta\omega\sigma''} f^{\text{xc}}_{\kappa\lambda\sigma',\eta\omega\sigma''}(X+Y)_{\kappa\lambda\sigma'}(X+Y)_{\eta\omega\sigma''} \right] \\
&= \frac{\partial}{\partial \xi} \left[\sum_g w_g \sum_{I,J} \frac{\partial^2 F}{\partial z_I \partial z_J} \bigg|_g u_J(\mathbf{P}) v_J(\mathbf{X}+\mathbf{Y}) u_I(\mathbf{P}) v_I(\mathbf{X}+\mathbf{Y}) + \sum_g w_g \sum_I \frac{\partial F}{\partial z_I} \bigg|_g u_I(\mathbf{X}+\mathbf{Y}) v_I(\mathbf{X}+\mathbf{Y}) \right] \\
&= \sum_g w_g^\xi \left[\sum_{IJ} \frac{\partial^2 F}{\partial z_I \partial z_J} \bigg|_g u_J(\mathbf{P}) v_J(\mathbf{X}+\mathbf{Y}) u_I(\mathbf{P}) v_I(\mathbf{X}+\mathbf{Y}) + \sum_I \frac{\partial F}{\partial z_I} \bigg|_g u_I(\mathbf{X}+\mathbf{Y}) v_I(\mathbf{X}+\mathbf{Y}) \right] \\
&\quad + \sum_g w_g \sum_{IJK} \frac{\partial^3 F}{\partial z_I \partial z_J \partial z_K} \bigg|_g u_K(\mathbf{P}) v_K(\mathbf{X}+\mathbf{Y}) u_J(\mathbf{P}) v_J(\mathbf{X}+\mathbf{Y}) z_I^{(\xi)}(\mathbf{P}) \\
&\quad + 2 \sum_g w_g \sum_{IJ} \frac{\partial^2 F}{\partial z_I \partial z_J} \bigg|_g u_J(\mathbf{P}) v_J(\mathbf{X}+\mathbf{Y}) [u_I^{(\xi)}(\mathbf{P}) v_I(\mathbf{X}+\mathbf{Y}) + u_I(\mathbf{P}) v_I^{(\xi)}(\mathbf{X}+\mathbf{Y})] \\
&\quad + \sum_g w_g \sum_{IJ} \frac{\partial^2 F}{\partial z_I \partial z_J} \bigg|_g u_J(\mathbf{X}+\mathbf{Y}) v_J(\mathbf{X}+\mathbf{Y}) z_I^{(\xi)}(\mathbf{P}) \\
&\quad + \sum_g w_q \sum_I \frac{\partial F}{\partial z_I} \bigg|_g [u_I^{(\xi)}(\mathbf{X}+\mathbf{Y}) v_I(\mathbf{X}+\mathbf{Y}) + u_I(\mathbf{X}+\mathbf{Y}) v_I^{(\xi)}(\mathbf{X}+\mathbf{Y})],
\end{aligned}$$

where w_g^ξ are the derivatives of the integration weights and the $z_I^{(\xi)}$, $u_I^{(\xi)}$, and $v_I^{(\xi)}$ are quantities that involve only basis function derivatives. These two exchange-correlation terms are computed together when the MOs Lagrangian is assembled so that the functional third derivatives are generated only once. The last exchange-correlation contribution to the excitation energy gradient involves only up to the second derivative of the functional and has the following form:

$$\begin{aligned}
V^{\text{xc}(\xi)}(\mathbf{P}^\Delta) &= \frac{\partial}{\partial \xi} \left[\sum_{\mu\nu\sigma} V^{\text{xc}}_{\mu\nu\sigma} P^{\Delta}_{\mu\nu\sigma} \right] \\
&= \frac{\partial}{\partial \xi} \left[\sum_{\mu\nu\sigma} \left(\sum_g w_g \sum_I \frac{\partial F}{\partial z_I} \bigg|_g u_I(\mathbf{P}) v_{I,\mu\nu} \right) P^{\Delta,\sigma}_{\mu\nu} \right] \\
&= \frac{\partial}{\partial \xi} \left[\sum_g w_g \sum_I \frac{\partial F}{\partial z_I} \bigg|_g u_I(\mathbf{P}) v_I(\mathbf{P}^\Delta) \right] \\
&= \sum_g w_g^\xi \left[\sum_I \frac{\partial F}{\partial z_I} \bigg|_g u_I(\mathbf{P}) v_I(\mathbf{P}^\Delta) \right] + \sum_g w_g \sum_{IJ} \frac{\partial^2 F}{\partial z_I \partial z_J} \bigg|_g u_J(\mathbf{P}) v_J(\mathbf{P}^\Delta) z_I^{(\xi)}(\mathbf{P}) \\
&\quad + \sum_g w_g \sum_I \frac{\partial F}{\partial z_I} \bigg|_g [u_I^{(\xi)}(\mathbf{P}) v_I(\mathbf{P}^\Delta) + u_I(\mathbf{P}) v_I^{(\xi)}(\mathbf{P}^\Delta)].
\end{aligned}$$

¹M. A. L. Marques and E. K. U. Gross, *Annu. Rev. Phys. Chem.* **55**, 427 (2004).

²M. E. Casida, in *Recent Advances in Density Functional Methods*, edited by D. P. Chong (World Scientific, Singapore, 1995) Pt. 1; E. U. K. Gross, J. F. Dobson, and M. Petersilka, in *Density Functional Theory II*, edited by R. F. Nalewajski (Springer, Heidelberg, 1996).

³E. R. Bitnner and D. S. Kosov, *J. Chem. Phys.* **110**, 6645 (1999).

⁴C. Van Caillie and R. D. Amos, *Chem. Phys. Lett.* **308**, 249 (1999); **317**, 159 (2000).

⁵F. Furche and R. Ahlrichs, *J. Chem. Phys.* **117**, 7433 (2004).

⁶S. Miertus, E. Scrocco, and J. Tomasi, *Chem. Phys.* **55**, 117 (1981).

⁷E. Cancès, B. Mennucci, and J. Tomasi, *J. Chem. Phys.* **107**, 3032 (1997); B. Mennucci, E. Cancès, and J. Tomasi, *J. Phys. Chem. B* **101**, 10506 (1997).

⁸V. Barone and M. Cossi, *J. Phys. Chem. A* **102**, 1995 (1998).

⁹A. Klamt and G. Schüürmann, *J. Chem. Soc., Perkin Trans. 2* **5**, 799 (1993).

¹⁰See Ref. 7 and B. Mennucci and R. Cammi, *Int. J. Quantum Chem.* **93**, 121 (2003).

¹¹See Ref. 7 and M. Cossi, V. Barone, B. Mennucci, and J. Tomasi, *Chem. Phys. Lett.* **286**, 253 (1998).

¹²R. Cammi, B. Mennucci, and J. Tomasi, *J. Phys. Chem. A* **104**, 5631 (2000).

¹³R. Cammi, S. Corni, B. Mennucci, and J. Tomasi, *J. Chem. Phys.* **122**, 104513 (2005).

¹⁴E. V. Tsiper, V. Chernyak, S. Tretiak, and S. Mukamel, *J. Chem. Phys.* **110**, 8328 (1999); S. Tretiak and S. Mukamel, *Chem. Rev. (Washington, D.C.)* **102**, 3171 (2002).

¹⁵J. Hutter, *J. Chem. Phys.* **118**, 3928 (2003).

¹⁶R. Car and M. Parrinello, *Phys. Rev. Lett.* **55**, 2471 (1985).

¹⁷J. Tomasi and M. Persico, *Chem. Rev. (Washington, D.C.)* **94**, 2027 (1994).

¹⁸C. J. Cramer and D. G. Truhlar, *Chem. Rev. (Washington, D.C.)* **99**, 2161 (1999).

¹⁹J. Tomasi, B. Mennucci, and R. Cammi, *Chem. Rev. (Washington, D.C.)* **105**, 2999 (2005).

²⁰A. D. Becke, *J. Chem. Phys.* **98**, 1372 (1993); **98**, 5648 (1993).

²¹G. Scalmani, V. Barone, K. N. Kudin, C. S. Pomelli, G. E. Scuseria, and M. J. Frisch, *Theor. Chem. Acc.* **111**, 90 (2004).

- ²² M. Cossi, G. Scalmani, N. Rega, and V. Barone, *J. Chem. Phys.* **117**, 43 (2002); M. Cossi, N. Rega, G. Scalmani, and V. Barone, *J. Comput. Chem.* **24**, 669 (2003).
- ²³ R. Bauernschmitt and R. Ahlrichs, *Chem. Phys. Lett.* **256**, 454 (1996); R. E. Stratmann, G. E. Scuseria, and M. J. Frisch, *J. Chem. Phys.* **109**, 8218 (1998); S. Hirata and M. Head-Gordon, *Chem. Phys. Lett.* **314**, 291 (1999).
- ²⁴ P. Jorgensen and J. Simons, *Second Quantization Based Methods in Quantum Chemistry* (Academic, New York, 1981).
- ²⁵ R. Cammi and B. Mennucci, *J. Chem. Phys.* **110**, 9877 (1999); M. Cossi and V. Barone, *ibid.* **115**, 4708 (2001).
- ²⁶ N. C. Handy and H. F. Schaefer III, *J. Chem. Phys.* **81**, 5031 (1984).
- ²⁷ R. G. Raffanetti, *Chem. Phys. Lett.* **20**, 335 (1973).
- ²⁸ J. B. Foresman, M. Head-Gordon, J. A. Pople, and M. J. Frisch, *J. Phys. Chem.* **96**, 135 (1992).
- ²⁹ J. E. Rice, R. D. Amos, N. C. Handy, T. J. Lee, and H. F. Schaefer III, *J. Chem. Phys.* **85**, 963 (1986).
- ³⁰ R. Cammi, B. Mennucci, and J. Tomasi, *J. Phys. Chem. A* **103**, 9100 (1999); R. Cammi, B. Mennucci, C. Pomelli, C. Cappelli, S. Corni, L. Frediani, G. W. Trucks, and M. J. Frisch, *Theor. Chem. Acc.* **111**, 66 (2004).
- ³¹ M. Cossi, B. Mennucci, and R. Cammi, *J. Comput. Chem.* **17**, 53 (1996).
- ³² M. E. Casida, F. Gutierrez, J. Guan, F.-X. Gadea, D. R. Salahub, and J.-P. Daudey, *J. Chem. Phys.* **113**, 7062 (2000); A. Dreuw, J. L. Weisman, and M. Head-Gordon, *ibid.* **119**, 2043 (2003).
- ³³ D. Rappoport and F. Furche, *J. Am. Chem. Soc.* **126**, 1277 (2004).
- ³⁴ R. Improta and V. Barone, *J. Am. Chem. Soc.* **126**, 14320 (2004); T. Gustavsson, A. Banyasz, E. Lazzarotto, D. Markovitsi, G. Scalmani, M. J. Frisch, V. Barone, and R. Improta, *ibid.* **128**, 607 (2006).
- ³⁵ M. J. Frisch, G. W. Trucks, H. B. Schlegel *et al.*, GAUSSIAN, Development Version, Revision D.02, Gaussian, Inc., Wallingford, CT, 2004.
- ³⁶ K. V. Mikkelsen, Y. Luo, H. Ågren, and P. Jørgensen, *J. Chem. Phys.* **100**, 8240 (1994); K. V. Mikkelsen and K. O. Sylvester-Hvid, *J. Phys. Chem.* **100**, 9116 (1996); S. P. Karna, P. N. Prasad, and M. Dupuis, *J. Chem. Phys.* **94**, 1171 (1991); C. Daniel and M. Dupuis, *Chem. Lett.* **171**, 209 (1990); F. Sim, S. Chin, M. Dupuis, and J. E. Rice, *J. Phys. Chem.* **97**, 1158 (1993); B. Champagne, *Chem. Phys. Lett.* **261**, 57 (1996); S. D. Bella, G. Lanza, I. Fragala, Sh. Yitzchaik, M. A. Ratner, and T. J. Marks, *J. Am. Chem. Soc.* **119**, 3003 (1997); J. L. Bredas and F. Meyers, *Nonlinear Opt.* **1**, 119 (1991); H. Ågren, O. Vahtras, H. Koch, P. Jørgensen, and T. Helgaker, *J. Chem. Phys.* **98**, 6417 (1993); D. Jonsson, P. Norman, H. Ågren, Y. Luo, K. O. Sylvester-Hvid, and K. V. Mikkelsen, *ibid.* **109**, 6351 (1998); C.-K. Wang, Y.-H. Wang, Y. Su, and Y. Luo, *ibid.* **119**, 4409 (2003).
- ³⁷ R. Cammi, L. Frediani, B. Mennucci, and K. Ruud, *J. Chem. Phys.* **119**, 5818 (2003).
- ³⁸ A. M. Moran, A. Myers Kelley, and S. Tretiak, *Chem. Phys. Lett.* **367**, 293 (2003).
- ³⁹ O. S. Khalil, C. J. Seliskar, and S. P. McGlynn, *J. Chem. Phys.* **58**, 1607 (1973); W. Liptay, in *Excited States*, edited by E. C. Lim (Academic, New York, 1974), Vol. 1, p. 129; M. Harrand, *J. Raman Spectrosc.* **2**, 15 (1974); **4**, 53 (1975); T. P. Carsey, G. L. Findley, and S. P. McGlynn, *J. Am. Chem. Soc.* **101**, 4502 (1979); J. N. Woodford, M. A. Pauley, and C. H. Wang, *J. Phys. Chem. A* **101**, 1989 (1997); C. L. Tomsen, J. Thøgersen, and S. R. Keiding, *ibid.* **102**, 1062 (1998).
- ⁴⁰ A. M. Moran and A. M. Kelley, *J. Chem. Phys.* **115**, 912 (2001).
- ⁴¹ S. Millefiori, G. Favini, A. Millefiori, and D. Grasso, *Spectrochim. Acta, Part A* **33**, 21 (1977).
- ⁴² H. K. Sinha and K. Yates, *Can. J. Chem.* **69**, 550 (1990).
- ⁴³ R. Wortmann, P. Kramer, C. Glania, S. Lebus, and N. Detzer, *Chem. Phys.* **173**, 99 (1993).
- ⁴⁴ S. A. Kovalenko, R. Schanz, V. M. Farztdinov, H. Hennig, and N. P. Ernstring, *Chem. Phys. Lett.* **322**, 200 (2000); S. A. Kovalenko, A. L. Dobryakov, J. Ruthmann, and N. P. Ernstring, *Phys. Rev. A* **59**, 2369 (1999); V. M. Farztdinov, R. Schanz, S. A. Kovalenko, and N. P. Ernstring, *J. Phys. Chem. A* **104**, 11486 (2000).
- ⁴⁵ A. E. Reed, L. A. Curtiss, and F. Weinhold, *Chem. Rev. (Washington, D.C.)* **88**, 899 (1988).
- ⁴⁶ A. Klamt, *J. Phys. Chem.* **99**, 2224 (1995).
- ⁴⁷ E. Lippert, W. Lüder, and H. Boos, in *Advances in Molecular Spectroscopy*, edited by A. Mangini (Pergamon, Oxford, 1962), pp. 443–457.
- ⁴⁸ See, for example, A. B. J. Parusel, W. Rettig, and W. Sudholt, *J. Phys. Chem. A* **106**, 804 (2002); Z. R. Grabowski, K. Rotkiewicz, and W. Rettig, *Chem. Rev. (Washington, D.C.)* **103**, 3899 (2003) and references therein.
- ⁴⁹ K. Rotkiewicz, K. H. Grellmann, and Z. R. Grabowski, *Chem. Phys. Lett.* **19**, 315 (1973); Z. R. Grabowski, K. Rotkiewicz, A. Siemarczuk, D. J. Cowley, and W. Baumann, *Nouv. J. Chim.* **3**, 443 (1979).
- ⁵⁰ K. A. Zachariasse, T. von der Haar, A. Hebecker, U. Leinhos, and W. Kuhnle, *Pure Appl. Chem.* **65**, 1745 (1993); W. Schuddeboom, S. A. Jonker, J. H. Warman, U. Leinhos, W. Kuhnle, and K. A. Zachariasse, *J. Phys. Chem.* **96**, 10809 (1992).
- ⁵¹ B. Mennucci, A. Toniolo, and J. Tomasi, *J. Am. Chem. Soc.* **122**, 10621 (2000).
- ⁵² P. Gedeck and S. Schneider, *J. Photochem. Photobiol., A* **105**, 165 (1997); **121**, 7 (1999).
- ⁵³ Gas-phase experimental data have been measured through electron energy loss (EEL) experiments in C. Bulliard, M. Allan, G. Wirtz, E. Haselbach, K. A. Zachariasse, N. Detzer, and S. Grimme, *J. Phys. Chem. A* **103**, 7766 (1999), while experimental data in solution have been taken from Ref. 47.